JCTC Journal of Chemical Theory and Computation

Quantum Electronic Structure

A range-separated double-hybrid functional from nonempirical constraints

Eric Bremond, Marika Savarese, Ángel José Pérez-Jiménez, Juan Carlos Sancho-García, and Carlo Adamo

J. Chem. Theory Comput., **Just Accepted Manuscript** • DOI: 10.1021/acs.jctc.8b00261 • Publication Date (Web): 20 Jun 2018

ACS Publications

is published by the American Chemical Society. 1155 Sixteenth Street N.W., Washington, DC 20036

A range-separated double-hybrid functional from nonempirical constraints

Éric Brémond[1,*], Marika Savarese[2], Ángel José Pérez-Jiménez[3], Juan Carlos Sancho-García[3], and Carlo Adamo[4,5*]

Université Paris Diderot, Sorbonne Paris Cité, ITODYS, UMR CNRS 7086, 15 rue J.-A. de Baïf, F-75013 Paris, France; CompuNet, Istituto Italiano di Tecnologia, via Morego 30, I-16163 Genoa, Italy; Departamento de Química Física, Universidad de Alicante, E-03080 Alicante, Spain and Chimie ParisTech, PSL Research University, CNRS, Institut de Recherche de Chimie Paris, 11, rue Pierre et Marie Curie, F-75005 Paris, France ; Institut Universitaire de France, 103 Boulevard Saint Michel, F-75005 Paris, France.

Abstract

On the basis of our previous developments in the field of nonempirical double hybrids, we present here a new exchange-correlation functional based on a range-separated model for the exchange part and integrating a nonlocal perturbative correction to the electron correlation contribution. Named RSX-QIDH, the functional is free from any kind of empirical parameterization. Its range-separation parameter is set to recover the total energy of the hydrogen atom, thus eliminating the self-interaction error for this one-electron system. Subsequent tests on some relevant benchmark datasets confirm that the self-interaction error is particularly low for RSX-QIDH. This new functional provides also correct dissociation profiles for charged rare-gas dimers, and very accurate ionization potentials directly from Kohn-Sham orbital energies.

Above all, these good results are not obtained at the expense of other properties. Indeed, further tests on standard benchmarks show that RSX-QIDH is competitive with the more empirical ωB97X-2 double hybrid, and outperforms the parent LC-PBE long-range corrected hybrid, thus underlining the important role of the nonlocal perturbative correlation.

1)Université Paris Diderot ; 2) IIT ; 3) Universidad de Alicante ; 4) Chimie ParisTech; 5) IUF

*) Corresponding authors eric.bremond@univ-paris-diderot.fr, carlo.adamo@chimie-paristech.fr

1. Introduction

Among the plethora of methods based on Kohn-Sham density-functional theory (KS-DFT)[1], hybrid density functionals are undoubtedly the most widely used class of approximations to tackle the accurate modeling of chemical systems[2,3]. Based on the adiabatic connection model[4], they (partially) cure most of the KS-DFT issues that years of benchmarks and tests have clearly identified (for recent and detailed examples see references 5-7). Among others, the so-called self-interaction error (SIE)[8] arises, in one electron systems, from the non-cancellation of the spurious Coulomb self-repulsion energy by the approximate exchange-correlation contribution. More recently, the delocalization error (DE) was defined as a generalization of the many-electron SIE, thus suggesting that functionals with null DE are also SIE-free[9].

The introduction of a significant contribution of exact-like exchange (EXX) into the functional reduces the SIE. The resulting global hybrid (GH) functional contains a constant weight (i.e. electron-coordinate independent) of the EXX contribution which provides a non-negligible nonlocal character to the functional (and, of course, to the corresponding potential). This approach shows improved numerical accuracy in estimating a large number of physico-chemical properties such as reaction energy barriers[10,11] or optical spectra[12,13]. Global hybrids like B3LYP[14-16], PBE0[17,18] or those belonging to the Minnesota family[19], are among the most representative models.

Generally speaking, the exchange-correlation energy (E_{xc}) of a GH can be expressed as:

$$E_{xc}^{GH} = a_x E_x^{EXX} + (1 - a_x) E_x^{GGA} + E_c^{GGA} \quad (1)$$

where GGA stands for Generalized Gradient Approximation, one of the most used semilocal DFT approaches.

The fraction of EXX exchange, a_x, can be set on nonempirical basis[20,21] or by pragmatic fitting to reference chemical databases. EXX values typically range from 10 (as in TPSSh[22]) to 100% (as in M06-HF[23]). In practice, an EXX contribution between 20 and 40% is often required to balance the different sources of errors, but larger contributions are required in some cases. Among them, properties like ionization potentials (IPs)[24], bond-length alternations (BLAs) of long-conjugated chains[25] or long through-space charge-transfer excitations[26] are probably the most concerned. However, it is worth to note that a large excess can deteriorate other important properties, such as molecular structures[27].

From a more formal point of view, the exchange potential of a GH behaves in the asymptotic region as $-\frac{a_x}{r_{12}}$ thus not exactly recovering the correct behavior $-\frac{1}{r_{12}}$, r_{12} being the inter-electronic distance[28].

The concept of range-separated exchange (RSX), originally proposed by Savin[29], is a physically-sound solution to correct the asymptotic behavior of the exchange potential. Over the past few years, it has led to the development of several long-range corrected (LC) approaches, such as LC-PBE[30], LC-ωPBE[31] or ωB97[32], just to mention some of the most popular. For these functionals, the EXX contribution ranges between 0% and 100% at short and long inter-electronic distances, respectively. In the original LC scheme, the junction between short- and long-range regions is assured by the *erf* function and tuned by a parameter, ω[30]. The Coulomb-attenuating method (CAM)[33,34] is a generalization of the LC scheme, coupling a GH (such as B3LYP) at short r_{12} distance, with an high percentage of EXX at long r_{12} distance. These functionals provide low SIE, thus significantly improving a number of molecular properties, including dissociation limits for one-electron bound molecules, charge-transfer states or reaction energy barriers[35,36]. Among others, CAM-B3LYP[33], ωB97X[32] and M11[37] can be mentioned as representatives of the most recent RSX hybrids. The ω parameter is often determined on the basis of empirical criteria[30-33,35,37,38], even if some efforts have been done to determine it from physical arguments[39].

As for most of the hybridized density functionals, LC and CAM main limitation is related to the wrong description of weakly interacting systems, even if it is proved that they tend to better capture dispersion interactions than standard GHs[40,41]. This drawback is often overcome by coupling the range-separated scheme to a classical dispersion correction[40-43], even if the limits of the method clearly appear in some difficult cases[44,45].

A viable alternative consists in introducing nonlocal effects into the correlation contribution, using the so-called double-hybrid (DH) approximations[46-49]. DH functionals were introduced by Ernzerhof in 1996[50], firstly tested by Truhlar in 2004[51], and then later popularized by Grimme[52] by merging wavefunction and density-based approaches to get the best of both worlds. They sum to the self-consistent GH exchange-correlation energy (Eq. 1) a fraction of nonlocal correlation computed a posteriori according to the second-order perturbation theory (PT2), so that the exchange correlation energy can be expressed as:

$$E_{xc}^{DH} = a_x E_x^{EXX} + (1 - a_x)E_x^{GGA} + (1 - a_c)E_c^{GGA} + a_c E_c^{PT2} \quad (2)$$

where a_c governs the fraction of nonlocal PT2 correlation. In line with GHs, the a_x and a_c coefficients can be set by empirical construction (see for instance B2-PLYP[52] as

representative case) or by theoretical arguments founded on the adiabatic connection model[4] and exemplified by PBE0-DH[53,54] and PBE-QIDH[55] functionals. From a conceptual point of view, these latter functionals are particularly appealing, since they well show how the increase of physical constraints, with respect to the parent GGA (PBE[56]) and GH (PBE0[17,18]) functionals, leads to an improvement of the performances over a wide range of properties[57,58]. Furthermore, the increased contribution of nonlocal EXX (~ 70% in PBE-QIDH), imposed by the fulfillment of defined theoretical constraints, leads also to a global reduction of the SIE[55].

In this context, the next natural step is the introduction of the range-separated scheme within a double-hybrid functional in order to cumulate the advantages of both approaches. Originally developed by Ángyán and co-workers[59], this approach evolved a few years later with the development of the ωB97X-2 functional[60]. This latter is an excellent method to target the modeling of systems especially prone to SIE and to model weak interactions (see for instance references 61 and 62). As part of the ωB97 family[32], ωB97X-2 contains a significant number of empirical parameters (i.e. 16), a construction which often leads to improved performances for properties within the domain of training, but which is also source of numerical instabilities[63,64]. Other valuable efforts were focused on the range separation of the correlation energy mainly having in mind the treatment of weak van der Waals interactions[65,66].

Within this context, we propose in the present work to integrate a RSX scheme within our nonempirical 'quadratic-integrand double hybrid' (QIDH) model[55], using fully nonempirical arguments. This new model, named RSX-QIDH, is the first exchange range-separated double-hybrid functional based on a simple and nonempirical exchange-correlation expression developed in a parameter-free fashion to solely satisfy physical constraints.

We show that by imposing two further theoretical conditions to the functional, i.e. the recovery of the correct asymptotic behavior of the exchange potential and of the hydrogen total energy, the resulting RSX-QIDH model allows to safely tackle challenging systems particularly prone to SIE that more standard exchange range-separated hybrids still fail to model.

2. The RSX-QIDH model

The starting point of the RSX-QIDH functional is the QIDH scheme[55] which is fully derived from the adiabatic connection[4]. In this framework, the exchange-correlation energy, E_{xc}, is defined as

$$E_{xc}[\rho] = \int_0^1 E_{xc,\lambda}[\rho] d\lambda \,, \tag{3}$$

where the coupling integrand $E_{xc,\lambda}$ is

$$E_{xc,\lambda} = \left\langle \Psi_\lambda \middle| V_{ee} \middle| \Psi_\lambda \right\rangle - \frac{1}{2} \iint dr' dr \frac{\rho(r)\rho(r')}{|r - r'|} \tag{4}$$

V_{ee} is the electron-electron interaction potential and Ψ_λ is the wavefunction minimizing the first term of Eqn.(4), under the constraint of producing a given density ρ. Three conditions can be defined for Eqn.(3). The first one is that for *λ=0:*

$$E_{xc,\lambda=0} = E_x^{EXX} \tag{5}$$

while the real interacting system corresponds to *λ=1* and it is described (here) by a given GGA approach:

$$E_{xc,\lambda=1} = E_{xc}^{GGA} \tag{6}$$

Another constraint is then introduced by considering the weak interaction limit (*λ→0*), where the first-order derivative of the integrand of Eqn.(3) is the second-order Görling-Levy (GL2) correlation energy[67], which could be approximated by a second-order perturbation term (PT2)

$$\left.\frac{\partial E_{xc,\lambda}}{\partial \lambda}\right|_{\lambda=0} = 2E_c^{GL2} \approx 2E_c^{PT2} \tag{7}$$

Eqn.(3) can be then solved using a simple dependency of $E_{xc,\lambda}$ upon *λ*:[68]

$$E_{xc,\lambda} = a[\rho] + b[\rho]\lambda + c[\rho]\lambda^2 \,, \tag{8}$$

where *a* and *b* are determined by respecting the conditions expressed by equations 5 and 6, while *c* is determined by the behavior of the integrand (1) close to the upper integral limit (λ=1)[55]. The resulting model, named Quadratic Integrand Double-Hybrid (QIDH)[55] is defined as:

$$E_{xc}^{QIDH,\alpha_x} = \frac{\alpha_x+2}{3} E_x^{EXX} + \frac{1-\alpha_x}{3} E_x^{GGA} + \frac{1}{3} E_c^{PT2} + \frac{2}{3} E_c^{GGA} \tag{9}$$

The α_x coefficient is determined following the linear-scaled one-parameter DH expression[54]:

$$a_c = a_x^3 \Rightarrow \frac{1}{3} = \left(\frac{\alpha_x+2}{3}\right)^3 \tag{10}$$

so that $a_x = 3^{-1/3}$ and $a_c = \frac{1}{3}$. The PBE-QIDH model is thus obtained by casting the PBE functional in Eqn.(9):

$$E_{xc}^{PBE-QIDH} = a_x E_x^{EXX} + (1 - a_x) E_x^{PBE} + (1 - a_c) E_c^{PBE} + a_c E_c^{PT2} \tag{11}$$

The self-consistent exchange-correlation 'quadratic-integrand hybrid' (QIH(SCF)) energy is derived from Eqn.(11) by neglecting the E_c^{PT2} contribution:

$$E_{xc}^{PBE-QIH(SCF)} = a_x E_x^{EXX} + (1 - a_x) E_x^{PBE} + (1 - a_c) E_c^{PBE} \tag{12}$$

The CAM approach consists in splitting the Coulomb interaction into a short- and a long-range (SR and LR, respectively) term[33]:

$$\frac{1}{r_{12}} = \frac{1-[\alpha+\beta f(\omega r_{12})]}{r_{12}} + \frac{\alpha+\beta f(\omega r_{12})}{r_{12}} \quad (13)$$

Where *f* is the error function (*erf*) in order to get analytic expressions of the bi-electronic integrals with a Gaussian basis set[30] and ω rules the long- and short-range separation. The α parameter determines the inclusion of an EXX contribution scaled by α over the whole r_{12} range, while β ruled the GGA exchange contribution scaled by a factor 1-(α+β). Please note that 0≤α+β≤1, 0≤α≤1 and 0≤β≤1[33]. Imposing β =1-α in Eqn.(13) assures the recovery of 100% of EXX at long interlectronic distance, thus constraining the right $-\frac{1}{r_{12}}$ asymptote for the exchange potential.

Setting α = a_x imposes the QIDH model for short interlectronic distances. The resulting RSX-QIDH thus reads:

$$E_{xc}^{RSX-QIDH} = a_x E_x^{EXX} + (1-a_x)E_x^{LR-EXX}(\omega) + (1-a_x)E_x^{PBE} - (1-a_x)E_x^{SR-PBE}(\omega) + (1-a_c)E_c^{PBE} + a_c E_c^{PT2} \quad (14)$$

where a_x = $3^{-1/3}$ and $a_c = \frac{1}{3}$, as above. As before, the self-consistent exchange-correlation RSX-QIH(SCF) energy is obtained by neglecting the perturbative contribution in Eqn.(14):

$$E_{xc}^{RSX-QIH(SCF)} = a_x E_x^{EXX} + (1-a_x)E_x^{LR-EXX}(\omega) + (1-a_x)E_x^{PBE} - (1-a_x)\,E_x^{SR-PBE}(\omega) + (1-a_c)E_c^{PBE} \quad (15)$$

The range-separated parameter, ω, is yet to be determined in order to fully define the functional. The most common way is to set this parameter in order to minimize the error with respect to a training dataset[30-33,37,38]. An alternative but system-dependent way, consists in determining ω from the fulfillment of the Koopmans' theorem, as done for the optimal tuned functionals[39], or as function of the electron density[69]. Here, following previous works[70,71], we determine ω by imposing an additional physical constraint, which is the exact treatment of the ground state energy of the hydrogen atom. Figures S1 and S2 report the variation of the RSX-QIDH total energy of the hydrogen atom with respect to the ω value, obtained with the Hartree-Fock (HF) or RSX-QIH(SCF) densities, respectively. In both cases, the minimum is obtained for ω =0.27 $bohr^{-1}$, a value not far from that used in ωB97X-2 (0.3 $bohr^{-1}$)[60]. For the sake of clarity, all the nonempirical parameters of the RSX-QIDH are reported in Table 1.

3. Computational details

All computations were performed with a locally modified version of the Gaussian program[72] in which the range-separated exchange quadratic-integrand hybrid and double hybrid (RSX-QIH(SCF) and RSX-QIDH, respectively) were fully implemented using the PBE exchange-correlation density functional[56] to evaluate the semilocal energy terms in Eq.(6). For comparison purposes, the range-separated double hybrid ωB97X-2[60], in its LP version, was also implemented in the same version of the software. In order to have a complete evaluation with other recent and commonly-used functionals, some computations were carried out with the ωB97X, and ωB97XD models, so to complete the ωB97 class[32], while the M06-HF, M06-2X and M11 functionals[23,37] were selected as representatives of the large Minnesota family.

The aug-cc-pVQZ basis set[73] was used to compute the dissociation profiles of the cationic dimers (H_2^+, He_2^+, $Ne_2^+$and Ar_2^+), while the def2-QZVP basis set[74] was considered for all the benchmarks concerning the Minnesota datasets[7]. Following previous recommendations[6], electron affinities (EA/13 dataset) were computed using the aug-def2-QZVP basis, obtained by adding diffuse s and p functions from the Dunning aug-cc-pVQZ[75] to def2-QZVP. To complete the investigation, the SIE4x4 and the IPK/7 datasets were also considered. The former is a recent evolution of the SIE11 dataset[76] and it probes systems particularly prone to SIE. The latter is composed by the experimental IPs of 7 molecules containing a double bond, Y=X (X=Si, C Y= N, P), bonded to hydrogen or methyl groups, so that the electronic properties depend on the X and Y atoms and on the substituents[77].

The delocalization error was estimated using the so-called "well-separated" He clusters[9,78]. They are planar rearrangements of He_n clusters (n=1 to 16) in which the atoms are distributed on a circle, two neighboring atoms being at 10 Å of distance. The delocalization error is then defined as the difference between the computed IP and the IP of a single He atom at the same level of theory[78].

4. Results and discussions

Choosing the parameter ω so to recover the total energy of the hydrogen atom, implies the cancellation of SIE for this one-electron system. It is interesting to verify, as first step, if this feature concerns also other systems affected by one- and many-electrons SIE. At the same time, a (full) correction of this error implies that the Kohn-Sham orbital energies should be closer to the corresponding IPs, within the Koopmans' theorem[79]. These points are discussed in some details in the next subsection. Then, the performances of the new RSX-QIDH functional are tested on a number of other molecular properties, in order to verify that the

improvements on the SIE-related systems have been not obtained at the expense of other and equally important properties. Finally, the role of the PT2 contribution is dissected by comparing RSX-QIDH and RSX-QIH(SCF) results.

4.1 Self-interaction error, ionization potentials and delocalization error.

As a first step in the assessment of the RSX-QIDH performances, we consider 4 ionized dimers for which the one-electron SIE has been clearly evidenced, namely H_2^+, He_2^+, Ne_2^+ and Ar_2^+. Indeed, as pointed a few years ago for H_2^+[80], standard functionals give an incorrect dissociation limit with a spurious charge delocalization on the two atoms at large interatomic distances[60,81]. As can be seen from the plots of Figure 1, the RSX-QIDH energy profile has not only the correct qualitative behavior with no dissociation barrier, but it is also practically coincident to that obtained with ωB97X-2 and it is very close to the exact HF curve. The other RSX hybrid functionals also have a correct behavior, but the dissociation limit is significantly underestimated, thus clearly indicating that their SIE errors are only partially compensated by the EXX contributions. Table 2 collects the differences in energy between X_2^+ and $X+X^+$ (X=H, He, Ne and Ar) obtained with different functionals at an interatomic distance of 100 Å. For H_2^+, RSX-QIDH has a value of -6.9 kcal/mol (10% of the energy minimum) lower than the correct HF reference, while ωB97X-2 gives -7.6 kcal/mol (about 12% of the corresponding energy minimum). A standard RSX functional like LC-PBE gives an error of -10.4 kcal/mol, significantly higher than that of PBE0 (-48.7 kcal/mol) or PBE (-66.0 kcal/mol). The B2-PLYP functional, which can be considered as the reference empirical DH, gives -31.3 kcal/mol[60].

Slightly more involved is the situation for the heavier dimers (i.e. He_2^+, Ne_2^+ and Ar_2^+) since also the nonlocal correlation plays a non-negligible role. Indeed for He_2^+ and Ne_2^+, all the considered functionals shows larger deviations with respect to the CCSD(T) reference. However, RSX-QIDH is still the best performer, followed by LC-PBE and ωB97X, respectively. In particular, the RSX-QIDH asymptote is -8.8 kcal/mol lower that the reference value (15% of the corresponding energy minimum, see Table 2), significantly better than ωB97X-2 (-14.1 kcal/mol, 23%). Literature data indicate -44.0 kcal/mol for B2-PLYP[60]. More interesting, RSX-QIDH provides better results for He_2^+ than a recent local hybrid functional, constructed to be SIE-free[82]. Lower errors are observed for Ar_2^+ (see Figure 1 and Table 2). The RSX-QIDH profile is again the closest to the reference, showing a deviation at

100 Å of only -3.2 kcal/mol, more than one half that found for ωB97X-2 (-7.8 kcal/mol) and ten times lower than the value computed for B2-PLYP (-27.6 kcal/mol)[60,83].

It is worth to notice that literature data suggest that the parent QIDH scheme[55] already provides good results for He_2^+ and Ar_2^+, when coupled with the PBE functional[56] or the recent SCAN meta-GGA[84], albeit the correct asymptotic limit is apparently not reached (see Figure 4 in reference 85).

In the last years, some datasets were built to specifically tackle severe SIE-related issues. Among others, the recent SIE4x4 dataset collects the interactions energies of four cationic dimers (H_2^+, He_2^+, $(NH_3)_2^+$, and $(H_2O)_2^+$) at different inter- atomic or molecular distances, for a total of 23 energy evaluations[6]. The results obtained with the selected functionals are reported in Figure 2. On this dataset, the RSX-QIDH approach provides a Mean Absolute Deviation (MAD) of 1.9 kcal/mol. All the other functionals show larger errors, encompassed between 4.7 and 13.4 kcal/mol (ωB97XD and ωB97X-2, respectively). An even better picture of the RSX-QIDH performances is obtained by analyzing the data reported in a very recent test on 217 functionals[6]. Here the lowest error on the SIE4x4 dataset is found for the combination of DSD-PBEP86 with the D3(BJ) classical dispersion correction[86], which gives a MAD of 5.0 kcal/mol, a value more than two times higher than that found for RSX-QIDH. Other DHs provide even larger errors. For instance, the deviation for B2-PLYP is 9.9 kcal/mol and 6.5 kcal/mol for B2GP-PLYP[60].

Another advantage of adopting the range-separated exchange is its accuracy in estimating IPs directly from Kohn-Sham orbital energies, since RSX functionals approximately satisfy the Koopmans' theorem[79]. Figure 4 reports the results on the IPK/7 dataset, which we have already used some years ago for some tests on SIE[77]. Here, the best accuracy is obtained with ωB97X, LC-ωPBE and RSX-QIDH, all providing a MAD around 7.0 kcal/mol. Significantly larger errors are shown by ωB97X-2 and LC-ωPBE (about 11 kcal/mol in both cases). Performances similar to RSX-QIDH are obtained with other RSX hybrid approaches, specifically tuned on IPs or SIE-prone systems, such as cam-QTP-00 (MAD=7.1 kcal/mol), LC-PR-BOP (MAD=3.9 kcal/mol) and scOT-RSH (MAD=4.6 kcal/mol)[87,88]. The good performances for IPs have been also verified on the IP/13 dataset, where the values are computed in an adiabatic fashion, as the energy difference between the neutral and cationic molecules. The good performance of the RSX-QIDH functional is confirmed, with a MAD close to those observed for ωB97X and ωB97XD. In addition, the deviations are significantly lower than those obtained for most of the functionals considered in a recent benchmark[7]. For

instance the M05, M06 and M08 families of functionals show deviations ranging between 2.8 (M05) and 3.8 (M06-HF) kcal/mol[7]. Other functionals give even larger deviations: CAM-B3LYP, 4.7 kcal/mol, PBE0 3.2 kcal/mol B3LYP 4.8 kcal/mol[7].

Strictly related to the SIE is the so-called delocalization error, which represents the unphysical over-delocalization of electrons and it is associated to the non-linear behavior of the total energy as function of the fractional electron occupation[9]. However, as pointed out by Yang and co-workers, a functional with null DE is SIE-free, but the reverse is not necessarily true[9]. A simple way to estimate DE is to evaluate the difference between the computed IPs of "well-separated" He clusters and the IP of a single He atom[9]. This difference increases with the cluster size and it is very large for local and semilocal functionals. Indeed, their typical errors are between 3 and 8 eV[78], due to the large delocalization of the positive hole created upon ionization over the whole cluster. As shown in Figure 3, the IP curves decrease as a function of the He_n cluster size until reaching a plateau. The deviation with respect to the reference is particularly small for M06-HF and RSX-QIDH. All other functionals have a significantly different behavior, the worst being the semilocal PBE approach. As a general trend, the DE decreases in going from semilocal to hybrids functionals and, in particular, the inclusion of range-separated exchange has a drastic effect on the deviations. Indeed, CAM-B3LYP provides a very low error (-4.33 eV) with respect to the parents BLYP (-8.09 eV) and B3LYP (-6.31 eV). The high ratio of EXX (~ 70 %) in the QIDH model already assures a small deviation for PBE-QIDH (-2.03 eV), an error which is further reduced in RSX-QIDH (-0.93 eV). The DE is not null as in the sophisticated Multi-Configuration Pair-DFT (MC-PDFT) approach and it is slightly higher than in M06-HF, which contains 100% of EXX (-0.67 eV)[78]. In short, the RSX-QIDH functional provides improved performances on a number of properties related to the SIE and DE. These performances are competitive with respect to similar approaches, parametrized or tuned on specific properties.

4.2 Other molecular properties

In order to check that the very encouraging results reported in the previous section are not obtained at the expense of other properties relevant for chemical applications, and to have a comparison with recent and commonly used functionals, we have carried out some further tests using representative datasets[7]. Table 3 collects the MADs obtained for all the considered functionals and datasets. Looking at the whole performance of each functional (MADs label "Total" in Table 3) it clearly appears that ωB97X-2 and RSX-QIDH perform significantly better than the other range-separated hybrids based on PBE. Both of them are also competitive

with the recent M11, which has having 44 parameters fitted to most of the datasets reported in Table 3 [37]. These three functionals are slightly worse than the robust M06-2X.

However, some significant differences appear looking at the results of the different datasets. Starting from the most classical benchmark, that is atomization energies (AE/6 dataset), the RSX-QIDH model outperforms the LC-PBE long-range corrected hybrid by 8.3 kcal/mol but performs less well than the LC-ωPBE variant by 1.7 kcal/mol. With respect to parametrized RSX hybrids (ωB97X and ωB97XD) and the ωB97X-2 double hybrid, the RSX-QIDH model remains less accurate by 3 to 4 kcal/mol. The same holds if M06-2X and M11 are considered (see Table 3). Such an unfavorable trend on atomization energy properties was already observed in a previous investigation regarding nonempirical global hybrids and double hybrids, and was underlined as the consequence of the underpinning PBE semilocal functional[57]. This is, indeed, true for the PBE-QIDH approach[55,85] and the situation is even worst when the recent SCAN functional is considered in the QIDH model[85]. Furthermore, it should be noticed that ωB97X-2 remains also less accurate than its parent hybrids.

A significant improvement is, in contrast, observed for bond dissociation energies (ABDE/4 dataset), where RSX-QIDH provides lower deviations than the other range-separated density functionals, with a MAD of 1.4 kcal/mol. The ωB97X-2 functional shows an error of 2.6 kcal/mol, close to that of ωB97X and ωB97XD (2.4 and 2.6, in the order). It is noteworthy to point out that for the ABDE/4 dataset, RSX-QIDH is better than 76 functionals (out of 77) reported in a recent extensive investigation, also including the Minnesota functionals from ’05 to ’11 millesimal, and some of the most-common RSX hybrids, such as CAM-B3LYP[7]. The exception is represented by the M06-2X which gives a very low error (0.8 kcal/mol, see Table 3).

Such a comparison can be extended to recently developed functionals such as the B97M-V[89] and ωB9M-V[90]. The former is a meta-GGA approach, while the latter is its range-separated evolution. Both functionals are coupled with a dispersion correction and their numerous parameters were determined using a careful combinatorial optimization on many properties, including most of those present in our benchmark. Even if a direct comparison cannot be done since these functionals were benchmarked on different data sets, it is worth to notice that B97M-V performs less well than M06-2X and ωB97XD on bond dissociation energies, ωB9M-V shows a similar error[90]. It could be then inferred that RSX-QIDH provides similar results to ωB9M-V on this property.

Regarding proton affinities (PA/8 dataset), the RSX-QIDH model confirms its first position with respect to the other functionals considered in the present paper. Furthermore, its performance (1.2 kcal/mol) is comparable to those obtained by recent functionals, such as M11 (1.0 kcal/mol), M08-HX (1.1 kcal/mol)[7] or SCAN-QIDH (1.2 kcal/mol)[85] and better than B97M-V (3.0 kcal/mol) which includes proton affinities in its training set[89].

Analogously, dipole interactions (DI/6 dataset) are also accurately reproduced at the RSX-QIDH level, with a MAD comparable to that obtained with ωB97D or M06-2X (0.27 vs. 0.25 kcal/mol). Once again, literature data show that similar accuracies (0.22-0.27 kcal/mol) are obtained only by the Minnesota functionals (M05, M05-2X, M06, M08-HX), all the other standard functionals providing larger deviations[7].

Regarding the HAT/6, UA/6 and HT/6 datasets, the addition of nonlocal correlation decreases systematically the mean absolute deviation of the RSX-QIDH model with respect to LC-PBE with variations ranging from 0.2 to 2.2 kcal/mol. The same behavior is observed for ωB97X-2 with respect to ωB97X, but both these functionals provide errors lower than RSX-QIDH. This is particularly evident for HAT/6 where this latter functional gives a MAD of 3.2 kcal/mol, while ωB97X-2 result is 1.1 kcal/mol. Even better accuracy is obtained at M06-2X or M11 level (0.6 and 0.7 kcal/mol, respectively) while M06-HF is less accurate than RSX-QIDH (4.3 kcal/mol). A comparison with other recent functionals suggests that RSX-QIDH provides an accuracy on hydrogen transfer reaction similar to that found at PBE-QIDH or SCAN-QIDH level[85], but significantly better than B97M-V or ωB97X-D, this latter being less accurate than M06-2X[90].

A larger effect of nonlocal correlation is, instead observed for another class of reactions, the nucleophilic substitution (NS/6 dataset), where RSX-QIDH gives 1.9 kcal/mol, a value lower than those obtained with most of all the other functionals, except ωB97XD (1.2 kcal/mol), M06-2X (1.3 kcal/mol) and M11 (1.4 kcal/mol).

The positive effect of the nonlocal PT2 correlation is also observed for the EA/13 and HB/6 datasets, where a decrease of the error is found in going from LC-PBE to RSX-QIDH. However, the result for the EA dataset is disappointing, the MAD being as high as 2.8 kcal/mol. If this value is lower than that obtained at the ωB97X-2 level (3.2 kcal/mol), it remains significantly higher than the best results of our benchmark (M11, 0.7 kcal/mol). However, similar values have been obtained for other commonly-used functionals, such as M06-HF (2.6 kcal/mol), PBE0 (2.8 kcal/mol)[7] and ωB97M-V (2.2 kcal/mol)[90]. Only for electron affinities (EA/13 dataset), the RSX-QIDH model performs not as well as the parent

long-range corrected hybrids, but this behavior is also observed in the case of empirical approaches of the ωB97 family, including B97M-V and ωB97M-V[90].

The results on the charge transfer dataset (CT/7) show that LC-PBE and RSX-QIDH have the same accuracy (0.5 kcal/mol), higher than that offered by ωB97X-2 (1.0 kcal/mol), but lower than that found for ωB97X (0.4 kcal/mol) or ωB97XD (0.3 kcal/mol). The performances of RSX-QIDH are close to that provided by CAM-B3LYP (0.5 kcal/mol)[7], M06-HF (0.6 kcal/mol), while standard GHs like PBE0 and B3LYP give higher deviations (1.1 and 0.7 kcal/mol, respectively)[7]. Others Minnesota functionals, such as M11 and M06-2X, are slightly more accurate, with deviations of 0.6 and 0.8 kcal/mol, respectively (see Table 3). On this property the recent ωB97M-V functional is particularly performing, showing an error as low as 0.1 kcal/mol[90].

Finally, a particular attention is given to weak interactions, here represented by two datasets, namely WI/7 and PPS/5. The RSX-QIDH errors are 0.2 and 0.3 kcal/mol, respectively. The ωB97X model provides a lower error for the former dataset (WI/7, 0.1 kcal/mol), but, unexpectedly, the deviation increases after the inclusion of nonlocal correlation (ωB97X-2, 0.2 kcal/mol). This behavior could be related to the larger contribution of EXX in the functional, which overcomes the PT2 treatment of dispersion forces. The π-π interactions are, instead not affected by this contribution, the MAD being always about 0.4 kcal/mol for all the three functionals of the ωB97X family. More in general, it should be pointed out that the RSX-QIDH functional is among the few approaches to provide low deviations on both WI/7 and PPS/5. Indeed, most of the functionals are unbalanced towards one of the two datasets. For instance, PBE is particularly good on the first set (MAD of 0.1 kcal/mol) but not particularly accurate on the second (2.2 kcal/mol)[7]. A similar behavior is observed for PBE0 (0.1 and 1.7 kcal/mol, respectively) and CAM-B3LYP (0.1 and 1.9 kcal/mol), just to mention few examples.

Functionals belonging to the Minnesota family provide a similar error on the two datasets, albeit with slightly higher variations (see Table 3 and reference 7), while B97M-V and ωB97M-V, both containing a dispersion correction, are particularly accurate on the large S22 and S66 datasets[90]. For all these functionals, however, dispersion interactions were also included in the training sets.

In order to have more insights on model systems for weak interactions and to complete the investigation started with the cationic rare-gas dimers, the dissociation energy profiles of the He_2, Ne_2 and Ar_2 dimers have been also considered. The results are plotted in Figure 4, where

CCSD(T) data are taken as reference. The dissociation curves for He_2 are encompassed by the repulsive profile of LC-PBE, which does not show any energy minimum, and the very attractive potential of ωB97X-2 which is more than 5 times deeper than the reference (-0.11 vs. -0.02 kcal/mol). This behavior suggests a double counting of the electron correlation, due to the large PT2 contribution in the functional. RSX-QIDH shows an attractive minimum, even if the energy is quite low (-0.01 kcal/mol) with respect to ωB97X (-0.02 kcal/mol), this latter being very close to the CCSD(T) reference. This trend is also observed for the other two dimers (Ne_2 and Ar_2): LC-PBE is always repulsive, the ωB97X-2 functional significantly overbinds and RSX-QIDH gives a shallow description of the minima. The ωB97X is always the closest to the reference. Taken together, these results well underline how the RSX-QIDH gives fairly good performances on a number of molecular properties of interest for chemical applications.

4.3 On the role of the PT2 contribution

From the above reported data, it could be argued that, for some datasets, the larger EXX contribution predominantly rules the performances of the RSX-QIDH functional, confining the nonlocal PT2 correlation to a subsidiary part. In order to investigate this effect, we have carried out some computations using the RSX-QIH(SCF) functional defined by Eq. (6), which does not contain the PT2 contribution. The obtained results are reported in Figure 5 and clearly illustrates how the nonlocal PT2 contribution strongly affects all the considered properties, with a large increase of the errors in going from RSX-QIH(SCF) to RSX-QIDH. This is particular evident for some datasets, where nonlocal correlation is expected to play a major role: AE/6 (+ 246%), ABDE/4 (+939 %), HAT/6 (+270 %), PPS/5 (+432 %). The only exception in this general trend is represented by the hydrogen bond energies (HB/6), which are better reproduced at the RSX-QIH(SCF) level than at RSX-QIDH (-200 %). The negative effect of the nonlocal PT2 correlation can be also observed in going from ωB97XD to ωB97X-2, where the MAD on the HB/6 dataset increases from 0.25 to 0.75 (+300 %). A similar behavior is present in the PBE0 and PBE-QIDH functionals[57,85].

In short, the inclusion of nonlocal PT2 correlation has a beneficial effect on almost all the properties.

5. Conclusions and perspectives

In the present paper, we propose a new nonempirical functional, RSX-QIDH, based on two well-established models, namely the exchange-range separation and the nonlocal electron correlation. Based on strong physical arguments, the proposed functional contains an additional parameter, ruling the short- and long-range electron separation in the exchange, which is chosen so to recover the total energy of the hydrogen atom. The cancellation of one-electron self-interaction error and the restoration of the correct $-\frac{1}{r_{12}}$ behavior in the potential have a beneficial effect on some difficult cases, such as the dissociation profiles of cationic rare-gas dimers and the ionization potentials directly evaluated from Kohn-Sham orbital energies. Further tests on standard molecular benchmarks show that RSX-QIDH performs at least as well as more empirical range-separated hybrids, eventually including nonlocal PT2 correlation term.

Pleasant characteristics of this functional are its numerical stability and high-order derivability envisaging its use for a number of properties.

Of note, and as for the vast majority of the functionals developed up to now, the domain of applicability of this functional is linked to the benchmark sets considered. This opens some questions, for instance, concerning its extensibility to periodic systems, which are scarcely represented in the current benchmark sets. In general and up to now the question of an exchange-correlation functional describing on an equal foot molecules and solids is still open. Different functionals seem to work for several properties[91]. For instance, GGA functionals are more suitable to describe metallic solids, while they fail for some properties (e.g. gap) of semiconductors. The opposite is true for GHs. Screened hybrid density functionals, such as HSE[92], significantly improve gaps, but not necessarily structural parameters[93]. The few tests carried out with RSXs are somehow contradictory[94,95]. Double hybrids are probably unsuitable for metallic solids[96], due to divergence problems that could derive from the PT2 terms but they are rather promising for molecular crystals (see for instance reference 97). A recent paper proposed a RSX-DH approach applied to solids and the results are encouraging, albeit only a few systems were tested[98]. Since efficient implementations of perturbative approach within Periodic Boundary Conditions were done both with Gaussian and planewave basis sets[99,100], opening the perspectives of more systematic tests of both DHs and RSX-DHs functionals, we expect that a definitive answer on their use for solid state could be assessed in the near future.

Acknowledgement

E.B. gratefully acknowledges the GENCI-CINES for HPC resources (Projects AP010810360 and A0040810359).

Supporting information

The Supporting Information is available free of charge on the ACS Publications website: variation of the total energy of the hydrogen atom as function of the ω parameter, raw data of Table 3 and Figures 1 to 5.

References

1) Kohn, W.; Sham, L. J. Self-consistent Equations Including Exchange and Correlation Effects. *Phys. Rev.* **1965**, *140*, A1133.

2) Becke, A.D. Fifty years of density functional theory in chemical physics *J. Chem. Phys*. **2014**, *140*, 18A301.

3) Cohen, A.J. Mori-Sánchez, P.; Yang; W. Challenges for Density Functional Theory *Chem. Rev*. **2012**, *112*, 289–320

4) Harris, J. Adiabatic-connection Approach to Kohn-Sham Theory. P*hys. Rev. A: At., Mol., Opt. Phys*. **1984**, *29*, 1648-1659.

5) Mardirossian, N.; Head-Gordon M. Thirty Years of Density Functional Theory in Computational Chemistry: An Overview and Extensive Assessment of 200 Density Functionals. *Mol. Phys*. **2017**, *119*, 2315-2372.

6) Goerigk, L.; Hansen, A.; Bauer, C.; Ehrlich, S.; Najibi, A.; Grimme, S. A Look at the Density Functional Theory Zoo with the Advanced GMTKN55 Database for General Main Group Thermochemistry, Kinetics and Noncovalent Interactions. *Phys. Chem. Chem. Phys.* **2017**, *19*, 32184-32215.

7) Peverati, R.; Truhlar, D. G. Quest for a Universal Density Functional: The Accuracy of Density Functionals Across a Broad Spectrum of Databases in Chemistry and Physics. *Phil. Trans. R. Soc. A* **2014**, *372*, 20120476.

8) Perdew, J. P.; Zunger, A. Self-interaction Correction to Density-functional Approximations for Many-electron Systems. *Phy. Rev. B* **1981**, *23*, 5048.

9) Li, C.; Zheng, X.; Su, N. Q.; Yang, W. Localized Orbital Scaling Correction for Systematic Elimination of Delocalization Error in Density Functional Approximations. *Nat. Sci. Rev.* **2017**, *5*, 203–215

10) Lynch, B. J.; Truhlar, D. G. How Well Can Hybrid Density Functional Methods Predict Transition State Geometries and Barrier Heights? *J. Phys. Chem. A* **2001**, *105*, 2936-2941

11) Mangiatordi, G. F.; Brémond, É.; Adamo, C. DFT and Proton Transfer Reactions: A Benchmark Study on Structure and Kinetics. *J. Chem. Theory Comput.* **2012**, *8*, 3082-3088.

12) Silva-Junior, M.R.; Schreiber, M.; Sauer, S.P., Thiel W. Benchmarks for Electronically Excited States: Time-dependent Density Functional Theory and Density Functional Theory Based Multireference Configuration Interaction. *J. Chem. Phys*. **2008**, *129*, 104103.

13) Jacquemin, D.; Adamo, C. Computational Molecular Electronic Spectroscopy with TD-DFT. *Top. Curr. Chem*. **2016**, *368*, 347-375.

14) Becke, A. D. Density-functional Thermochemistry. III. The Role of Exact Exchange. J. *Chem. Phys.* **1993**, *98*, 5648-5652.

15) Barone, V.; Adamo, C. Theoretical Study of Direct and Water-assisted Isomerization of Formaldehyde Radical Cation. A Comparison Between Density Functional and Post-Hartree-Fock Approaches. *Chem. Phys. Lett.* **1994**, *224*, 432-438.

16) Stephens, P. J.; Devlin, F. J.; Chabalowski, C. F. N.; Frisch, M. J. Ab initio Calculation of Vibrational Absorption and Circular Dichroism Spectra Using Density Functional Force Fields. *J. Phys. Chem.* **1994**, *98*, 11623-11627.

17) Adamo, C.; Barone, V. Toward Reliable Density Functional Methods Without Adjustable Parameters: The PBE0 Model. *J. Chem. Phys.* **1999**, *110*, 6158-6170.

18) Ernzerhof, M.; Scuseria, G. E. Assessment of the Perdew–Burke–Ernzerhof Exchange-correlation Functional. *J. Chem. Phys.* **1999**, *110*, 5029-5036.

19) Zhao, Y.; Truhlar, D. G. Density Functionals with Broad Applicability in Chemistry. *Acc. Chem. Res.* **2008**, *41*, 157-167.

20) Perdew, J. P.; Ernzerhof, M.; Burke, K. Rationale for Mixing Exact Exchange with Density Functional Approximations. *J. Chem. Phys.* **1996**, *105*, 9982-9985.

21) Guido, C. A.; Brémond, É.; Adamo, C.; Cortona, P. One Third: A New Recipe for the PBE0 Paradigm. *J. Chem. Phys.* **2013**, *138*, 021104

22) Staroverova, V. N.; Scuseria, G. E.; Tao, J.; Perdew, J. P. Comparative Assessment of a New

Nonempirical Density Functional: Molecules and Hydrogen-bonded Complexes. *J. Chem. Phys.* **2003**, *119*, 12129-12137.

23) Zhao, Y.; Truhlar D. G. The M06 Suite of Density Functionals for Main Group Thermochemistry, Thermochemical Kinetics, Noncovalent Interactions, Excited States, and Transition Elements: Two New Functionals and Systematic Testing of Four M06-class Functionals and 12 Other Functionals. *Theor. Chem. Acc.* **2006**, *120*, 215-241.

24) Lemierre, V.; Chrostowska, A.; Dargelos, A.; Chermette, H. Calculation of Ionization Potentials of Small Molecules: A Comparative Study of Different Methods. *J. Phys. Chem. A* **2005**, *109*, 8348-8355.

25) Jacquemin, D.; Adamo, C. Bond Length Alternation of Conjugated Oligomers: Wave Function and DFT Benchmarks. *J. Chem. Theory Comput.* **2010**, *7*, 369-376.

26) Dreuw, A.; Head-Gordon, M. Failure of Time-dependent Density Functional Theory for Long-range Charge-transfer Excited States: The Zincbacteriochlorin-bacteriochlorin and

Bacteriochlorophyll-spheroidene complexes. *J. Am. Chem. Soc.* **2004**, *126*, 4007-4016.

27) Brémond, É.; Savarese, M.; Su, N. Q.; Pérez-Jiménez, Á. J.; Xu, X.; Sancho-García, J. C.; Adamo, C. Benchmarking Density Functionals on Structural Parameters of Small-/Medium-sized Organic Molecules. *J. Chem. Theory Comput.* **2016**, *12*, 459-465.

28) Savin, A. On Degeneracy, Near-degeneracy, and Density Functional Theory. In *Recent Developments and Applications of Modern Density Functional Theory.* Seminario, J. M., Ed.; Elsevier: Amsterdam, Netherlands, 1996, 327-357.

29) Toulouse, J.; Colonna, F.; Savin, A. Long-range–short-range Separation of the Electron-electron Interaction in Density-functional Theory. *Phys. Rev. A* **2004**, *70*, 062505.

30) Iikura, H.; Tsuneda, T.; Yanai, T.; Hirao, K. A Long-range Correction Scheme for Generalized-gradient-approximation Exchange Functionals. *J. Chem. Phys.* **2001**, *115(8)*, 3540-3544.

31) Vydrov, O. A.; Heyd, J.; Krukau, A. V.; Scuseria, G. E. Importance of Short-range Versus Long-range Hartree-Fock Exchange for the Performance of Hybrid Density Functionals. *J. Chem. Phys.* **2006**, *125*, 074106.

32) Chai, J. D.; Head-Gordon, M. Systematic Optimization of Long-range Corrected Hybrid Density Functionals. *J. Chem. Phys.* **2008**, *128*, 084106.

33) Yanai, T.; Tew, D. P.; Handy, N. C. A New Hybrid Exchange-correlation Functional Using the Coulomb-attenuating Method (CAM-B3LYP). *Chem. Phys. Lett.* **2004***, 393*, 51-57.

34) Gill, P. M.; Adamson, R. D.; Pople, J. A. Coulomb-attenuated Exchange Energy Density Functionals. *Mol. Phys.* **1996**, *88*, 1005-1009.

35) Tawada, Y.; Tsuneda, T.; Yanagisawa, S.; Yanai, T.; Hirao, K. A Long-range-corrected Time-dependent Density Functional Theory. *J. Chem. Phys.* **2004**, *120*, 8425-8433.

36) Janesko, B. G.; Scuseria, G. E. Hartree-Fock Orbitals Significantly Improve the Reaction Barrier Heights Predicted by Semilocal Density Functionals. *J. Chem. Phys.* **2008**, *128*, 244112

37) Peverati, R.; Truhlar, D. G. Improving the Accuracy of Hybrid Meta-GGA Density Functionals by Range Separation. *J. Phys. Chem. Lett.* **2011**, *2*, 2810-2817.

38) Henderson, T. M.; Izmaylov, A. F.; Scalmani, G.; Scuseria, G. E. Can Short-range Hybrids Describe Long-range-dependent Properties? *J. Chem. Phys.* **2009**, *131*, 044108.

39) Baer, R.; Livshits, E.; Salzner, U. Tuned Range-separated Hybrids in Density Functional Theory. *Annu. Rev. Phys. Chem.* **2010**, *61*, 85-109.

40) Agrawal, P.; Tkatchenko, A.; Kronik, L. Pair-wise and Many-body Dispersive Interactions Coupled to an Optimally Tuned Range-separated Hybrid Functional. *J. Chem. Theory*

Comput. **2013***, 9*, 3473-3478.

41) Steinmann, S. N.; Corminboeuf, C. Comprehensive Benchmarking of a Density-dependent Dispersion Correction. *J. Chem. Theory Comput.* **2011**, *7*, 3567-3577.

42) Chai, J. D.; Head-Gordon, M. Long-range Corrected Hybrid Density Functionals with Damped Atom-atom Dispersion Corrections. *Phys. Chem. Chem. Phys.* **2008**, *10*, 6615-6620.

43) Sato, T.; Nakai, H. Density Functional Method Including Weak Interactions: Dispersion Coefficients Based on the Local Response Approximation. *J. Chem. Phys.* **2009**, *131*, 224104.

44) Steinmann, S. N.; Corminboeuf, C. Exploring the Limits of Density Functional Approximations for Interaction Energies of Molecular Precursors to Organic Electronics. *J. Chem. Theory Comput.* **2012**, *8*, 4305-4316.

45) Savarese, M.; Brémond, É.; Adamo, C. Exploring the Limits of Recent Exchange-correlation Functionals in Modeling Lithium/benzene Interaction. *Theor. Chem. Acc.* **2016**, *135*, 99.

46) Brémond, É.; Ciofini, I.; Sancho-García, J. C.; Adamo, C. Nonempirical Double-hybrid Functionals: An Effective Tool for Chemists. *Acc. Chem. Res.* **2016**, *49*, 1503-1513.

47) Su, N. Q.; Xu, X. The XYG3 Type of Doubly Hybrid Density Functionals. *WIREs: Comput. Mol Sci.* **2016**, *6*, 721-747.

48) Goerigk, L.; Grimme, S. Double-hybrid Density Functionals. *WIREs: Comput. Mol. Sci.* **2014**, *4*, 576-600.

49) Sancho-García, J. C.; Adamo, C. Double-hybrid Density Functionals: Merging Wavefunction and Density Approaches to Get the Best of Both Worlds. *Phys. Chem. Chem. Phys.* **2013**, *15*, 14581-14594.

50) Ernzerhof, M. Construction of the Adiabatic Connection. *Chem. Phys. Lett.* **1996**, *263*, 499-506.

51) Zhao, Y.; Lynch, B. J.; Truhlar, D. G. Doubly Hybrid Meta DFT: New Multi-Coefficient Correlation and Density Functional Methods for Thermochemistry and Thermochemical Kinetics. *J. Phys. Chem. A* **2004**, *108*, 4786-4791.

52) Grimme, S. Semiempirical Hybrid Density Functional with Perturbative Second-order Correlation. *J. Chem. Phys.* **2006**, *124*, 034108.

53) Brémond, É.; Adamo, C. Seeking for Parameter-free Double Hybrid Functionals: The PBE0-DH Model. *J. Chem. Phys.* **2011**, *135*, 024106.

54) Toulouse, J.; Sharkas, K.; Brémond, É.; Adamo, C. Rationale for a New Class of Double-hybrid Approximations in Density-functional Theory. *J. Chem. Phys.* **2011**, *135*, 101102.

55) Brémond, É.; Sancho-García, J. C.; Pérez-Jiménez, Á. J.; Adamo, C. Double-hybrid

Functionals from Adiabatic-connection: The QIDH Model. *J. Chem. Phys.* **2014**, *141*, 031101-031104.

56) Perdew, J. P.; Burke, K.; Ernzerhof, M. Generalized Gradient Approximation Made Simple. *Phys. Rev. Lett.* **1996**, *77*, 3865-3868

57) Brémond, É.; Savarese, M.; Pérez-Jiménez, Á. J.; Sancho-García, J. C.; Adamo, C. Systematic Improvement of Density Functionals Through Parameter-free Hybridization Schemes. *J. Phys. Chem. Lett.* **2015**, *6*, 3540-3545.

58) Brémond, É.; Savarese, M.; Pérez-Jiménez, Á. J.; Sancho-García, J. C.; Adamo, C. Speed-Up of the Excited-State Benchmarking: Double-Hybrid Density Functionals as Test Cases. *J. Chem. Theory Comput.* **2017**, *13*, 5539-5551.

59) Angyán, J. G.; Gerber, I. C.; Savin, A.; Toulouse, J. van der Waals Forces in Density Functional Theory: Perturbational Long-range Electron-interaction Corrections. *Physical Review A* **2005**, *72*, 012510.

60) Chai, J. D.; Head-Gordon, M. Long-range Corrected Double-hybrid Density Functionals. *J. Chem. Phys.* **2009**, *131*, 174105.

61) Klimeš, J.; Michaelides, A. Advances and Challenges in Treating van der Waals Dispersion Forces in Density Functional Theory. *J. Chem. Phys.* **2012**, *137*, 120901.

62) DeCarlos, E. T.; Ángyán, J. G.; Galli, G.; Zhang, C.; Gygi, F.; Hirao, K.; Song, J. W.; Rahul, K.; von Lilienfeld, O. A.; Podeszwa, R.; Bulik, I. W.; Henderson, T. M.; Scuseria, G. E.; Toulouse, J.; Peverati, R.; Truhlar, D. G.; Szalewicz, K. Blind Test of Density-functional-based Methods on Intermolecular Interaction Energies. *J. Chem. Phys.* **2016**, *145*, 124105.

63) Mardirossian, N.; Head-Gordon, M. How Accurate Are the Minnesota Density Functionals for Noncovalent Interactions, Isomerization Energies, Thermochemistry, and Barrier Heights Involving Molecules Composed of Main-Group Elements? *J. Chem. Theory Comput.* ***2016***, *12*, 4303-4325.

64) Goerigk, L. Treating London-Dispersion Effects with the Latest Minnesota Density Functionals: Problems and Possible Solutions. *J. Phys. Chem. Lett.* **2015**, *6*, 3891-3896.

65) Cornaton, Y.; Stoyanoca, A.; Jense, H.J.A.; Fromager, E. Altenative separation of exchange and correlation energies in range-separated density functional perturbation theory. *Phys. Rev. A* **2013**, *88*, 022516.

66) Zhang, I.Y.; Xu, X. Reaching a Uniform Accuracy for Complex Molecular Systems : Long_Range-Corrected XYG3 Doubly- Hybrid Density Functional. *J. Phys. Chem. Lett.* **2013**, *4*, 1669-1675.

67) Gorling, A; Levy, M. Correlation-energy functional and its high-density limit obtained

from a coupling-constant perturbation expansion. *Phys. Rev. B* **1993**, *47*, 13105-13113.

68) Cohen, A. J.; Mori-Sánchez, P.; Yang, W. Assessment and Formal Properties of Exchange-correlation Functionals Constructed from the Adiabatic Connection. *J. Chem. Phys.* **2007**, *127*, 034101.

69) Modrzejewski, M., Rajchel, L.; Chalasinski, G.; Szczesniak, M. M. Density-dependent Onset of the Long-Range Exchange: A Key to Donor-Acceptor Properties. *J. Phys. Chem. A* **2013**, *117*, 11580-11586.

70) Becke, A. D.; Johnson, E. R. A Simple Effective Potential for Exchange. *J. Chem. Phys.* **2006***, 124*, 221101.

71) Sun, J.; Ruzsinszky, A.; Perdew, J. P. Strongly Constrained and Appropriately Normed Semilocal Density Functional. *Phys. Rev. Lett.* **2015**, *115*, 036402.

72) Frisch, M. J.; Trucks, G. W.; Schlegel, H. B.; Scuseria, G. E.; Robb, M. A.; Cheeseman, J. R.; Scalmani, G.; Barone, V.; Petersson, G. A.; Nakatsuji, H.; Li, X.; Caricato, M.; Marenich, A. V.; Bloino, J.; Janesko, B. G.; Gomperts, R.; Mennucci, B.; Hratchian, H. P.; Ortiz, J. V.; Izmaylov, A. F.; Sonnenberg, J. L.; Williams-Young, D.; Ding, F.; Lipparini, F.; Egidi, F.; Goings, J.; Peng, B.; Petrone, A.; Henderson, T.; Ranasinghe, D.; Zakrzewski, V. G.; Gao, J.; Rega, N.; Zheng, G.; Liang, W.; Hada, M.; Ehara, M.; Toyota, K.; Fukuda, R.; Hasegawa, J.; Ishida, M.; Nakajima, T.; Honda, Y.; Kitao, O.; Nakai, H.; Vreven, T.; Throssell, K.; Montgomery, J. A., Jr.; Peralta, J. E.; Ogliaro, F.; Bearpark, M. J.; Heyd, J. J.; Brothers, E. N.; Kudin, K. N.; Staroverov, V. N.; Keith, T. A.; Kobayashi, R.; Normand, J.; Raghavachari, K.; Rendell, A. P.; Burant, J. C.; Iyengar, S. S.; Tomasi, J.; Cossi, M.; Millam, J. M.; Klene, M.; Adamo, C.; Cammi, R.; Ochterski, J. W.; Martin, R. L.; Morokuma, K.; Farkas, O.; Foresman, J. B.; Fox, D. J. *Gaussian 09, Revision E.1*, Gaussian, Inc., Wallingford CT, 2009.

73) Dunning, T. H.; Peterson, K. A.; Woon, D. E. Basis Sets: Correlation Consistent Sets. In *Encyclopedia of Computational Chemistry*; Schleyer, P. v. R., Ed.; John Wiley & Sons: New York, USA, 1999; 88-114.

74) Weigend, F.; Ahlrichs, R. Balanced Basis Sets of Split Valence, Triple Zeta Valence and Quadruple Zeta Valence Quality for H to Rn: Design and Assessment of Accuracy. *Phys. Chem. Chem. Phys.* **2005**, *7*, 3297-3305.

75) Kendall, R. A.; Dunning Jr, T. H.; Harrison, R. J. Electron Affinities of the First-row Atoms Revisited. Systematic Basis Sets and Wave Functions. *J. Chem. Phys.* **1992**, *96*, 6796-6806.

76) Goerigk, L.; Grimme, S. Efficient and Accurate Double-Hybrid-Meta-GGA Density

Functionals—Evaluation with the Extended GMTKN30 Database for General Main Group Thermochemistry, Kinetics, and Noncovalent Interactions. *J. Chem. Theory Comput.* **2010**, 6, 107-126.

77) Ciofini, I.; Chermette, H.; Adamo, C. A Mean-field Self-interaction Correction in Density Functional Theory: Implementation and Validation for Molecules. *Chem. Phys. Lett.* **2003**, *380*, 12-20.

78) Bao, J. L.; Wang, Y.; He, X.; Gagliardi, L.; Truhlar, D. G. Multiconfiguration Pair-Density Functional Theory Is Free From Delocalization Error. *J. Phys. Chem. Lett.* **2017**, *8*, 5616-5620.

79) Tsuneda, T.; Song, J. W.; Suzuki, S.; Hirao, K. On Koopmans' Theorem in Density Functional Theory. *J. Chem. Phys.* **2010**, *133*, 174101.

80) Chermette, H.; Ciofini, I.; Mariotti, F.; Daul, C. Correct Dissociation Behavior of Radical Ions such as H^{2+} in Density Functional Calculations. *J. Chem. Phys.* **2001**, *114*, 1447-1453.

81) Ruzsinszky, A.; Perdew, J. P.; Csonka, G. I. Binding Energy Curves from Nonempirical Density Functionals. I. Covalent Bonds in Closed-shell and Radical Molecules. *J. Phys. Chem A* **2005**, *109*, 11006-11014.

82) Schmidt, T.; Kraisler, E.; Makmal, A.; Kronik, L.; Kümmel, S. A Self-interaction-free Local Hybrid Functional: Accurate Binding Energies vis-à-vis Accurate Ionization Potentials from Kohn-Sham Eigenvalues. *J. Chem. Phys.* **2014**, *140*, 18A510.

83) It should be notice that our data obtained with the ωB97X-2 functional for Ne^{2+} and Ar^{2+} differ with respect to those reported in reference 60. In particular, the correct dissociation limit is not reached in both cases and no discontinuities are not found in the energy profiles. In contrast, the profiles are similar for H^{2+} and He^{2+}. These discontinuities arise, in our opinion, from broken symmetry solutions, where the charge is fully localized on one atom. This state leads to the correct dissociation limit, but it is higher in energy (40.6 kcal/mol at the equilibrium bond distance and ωB97X-2 level)

84) Sun, J.; Ruzsinszky, A.; Perdew, J.P. Strongly Constrained and Appropriately Normed Semilocal Density Functional *Phys. Rev. Lett*. **2015**, *115*, 036402.

85) Hui, K.; Chai, J.-D. SCAN-based hybrid and double-hybrid density functionals from models without fitted parameters. *J. Chem. Phys*. **2016**, *144*, 044114

86) Kozuch, S.; Martin, J. M. DSD-PBEP86: In Search of the Best Double-hybrid DFT with Spin-component Scaled MP2 and Dispersion Corrections. *Phys. Chem. Chem. Phys.* **2011**, *13*, 20104-20107.

87) Verma, P.; Bartlett, R. J. Increasing the Applicability of Density Functional Theory. IV.

Consequences of Ionization-potential Improved Exchange-correlation Potentials. *J. Chem. Phys.* **2014**, *140*, 18A534.

88) Tsuneda, T.; Hirao, K. Self-interaction Corrections in Density Functional Theory. *J. Chem. Phys.* **2014**, *140*, 18A513.

89) Mardirossian, N. Head-Gordon, M Mapping the genome of meta-generalized gradient approximation denity functionals: the search for B97M-V *J. Chem. Phys*. **2015**, *142*, 074111

90) Mardirossian, N. Head-Gordon, M. ωB97M-V : A combinatorially optimized, range-separated hybrid, meta-GGA density functional with VV10 nonlocal correlation, *J. Chem. Phys*. **2016**, *144*, 214110

91) Tran, F.; Stelzi, J.; Blaha, P. Rungs 1 to 4 of DFT Jacob's ladder: Extensive test on the lattice constant, bulk modulus and cohesive energy of solids. *J. Chem. Phys.* **2016**, *144*, 204120

92) Heyd, J.; Scuseria, G.E.; Ernzerhof, M. Hybrid functionals based on a screened Coulomb potential *J. Chem. Phys.* **2003**, 1*18*, 8207.

93) Labat, F.; Pouchan, C.; Adamo, C.; Scuseria, G.E. Role of Nonlocal Exchange in Molecular Crystals: The Case of Two Proton-ordered Phases of Ice, *J Comput. Chem*. **2011**, *32*, 2177–2185

94) Gerber, I.C.; Angyan, J.G.; Marsman, M.; Kresse, G. Range separated hybrid density functional with long-range Hartree-Fock exchange applied to solids, *J. Chem. Phys.* **2007**, *127*, 054101.

95) Matsushita, Y.; Nakamura, K.; Oshiyama, A. Comparative study of hybrid functionals applied to structural and electronic properties of semiconductors and insulators. *Phys. Rev. B*, **2011**, *84*, 075205.

96) Zhang, I.Y.; Rinke, P.; Perdew, J.P.; Scheffler, M. Towards Efficient Orbital-Dependent Density Functionals for Weak and Strong Correlation, *Phys. Rev. Lett.* **2016**, *117*, 133002.

97) Sharkas, K.; Toulouse, J.; Maschio, L.; Civalleri, B. Double-hybrids density-functional theory applied to molecular crystals *J. Chem. Phys.* **2014**, *141*, 044105

98) Sansone, G.; Civalleri, B.; Usvyat, D.; Toulouse, J.; Sharkas, K. ; Maschio, L. Range-separated double-hybrid density-functional theory applied to periodic systems *J. Chem. Phys.* **2015**, *143*, 102811

99) Pisani, C.; Busso, M.; Capecchi, G.; Casassa, S.; Dovesi, R.; Maschio, L.; Zicovich-Wilson, C.; Schütz, M. Local-MP2 electron correlation method for nonconducting crystals *J. Chem. Phys* **2005**, *122*, 094113.

100) Del Ben, M.; Hutter, J.; VandeVondele J. Second-Order Moller-Plesset Perturbation

Theory in the Consensed Phase: An Efficient and Massively Parallel Gaussian and Plane Waves Approach. *J. Chem. Theory Comput.* **2012**, *8*, 4177-4188.

Table 1. Nonempirical parameters used in the RSX-QIDH functional.

parameter	value	definition
a_x	$3^{-1/3}$	nonlocal EXX contribution (Eq. 6)
a_c	1/3	nonlocal PT2 contribution (Eq. 7)
α	$3^{-1/3}$	short/long range switching in $1/r_{12}$ term (Eq. 5)
ω	0.27	short/long range switching in erf function (Eq. 5)

Table 2. Deviations (kcal/mol) with respect to the correct dissociation asymptote for the H_2^+, He_2^+, Ne_2^+ and Ar_2^+ dimers computed at an interatomic distance of 100 Å.

dimer	PBE	PBE0	LC-PBE	ωB97X	ωB97X-2	RSX-QIDH
H_2^+	-66.0	-48.7	-10.4	-21.3	-7.6	-6.9
He_2^+	-94.6	-67.2	-24.8	-38.4	-14.3	-8.9
Ne_2^+	-96.3	-63.0	-28.3	-34.7	-17.1	-7.6
Ar_2^+	-62.0	-42.5	-5.5	-13.8	-7.8	-3.2

Table 3. Mean Absolute Deviations (MADs, kcal/mol) of selected hybrids, range-separated and double-hybrid functionals, computed on a representative benchmark dataset[7].

set[a]	LC-PBE	LC-ωPBE	M06-HF[b]	M06-2X[b]	M11[b]	ωB97X	ωB97XD	ωB97X-2	RSX-QIDH
AE/6	14.67	4.70	4.49	2.01	1.90	1.85	2.10	3.00	6.44
ABDE/4	3.06	5.06	5.01	0.81	1.67	2.42	2.58	2.61	1.38
EA/13	1.77	2.07	2.55	1.66	0.69	1.72	1.67	3.20	2.81
PA/8	1.60	2.22	2.81	1.69	1.03	2.00	2.87	2.34	1.18
HAT/6	3.45	2.22	4.32	0.62	0.73	2.13	1.92	1.13	3.17
NS/6	3.63	2.56	2.71	1.31	1.36	1.96	1.22	2.41	1.91
UA/6	2.42	2.09	1.79	1.03	1.47	2.30	1.98	0.96	1.80
HT/6	3.39	1.32	1.72	1.14	1.56	2.11	2.27	0.97	1.19
HB/6	1.03	0.74	0.59	0.33	0.29	0.76	0.25	0.75	0.86
CT/7	0.54	1.13	0.55	0.84	0.63	0.39	0.32	0.96	0.54
DI/6	0.31	0.85	0.50	0.25	0.44	0.45	0.25	0.71	0.27
WI/7	0.24	0.29	0.10	0.07	0.09	0.06	0.09	0.19	0.16
PPS/5	1.14	1.96	0.63	0.28	0.64	0.40	0.43	0.44	0.34
SIE4x4	6.94	9.35	4.20	8.63	9.55	11.36	13.37	4.71	1.91
IP/13	7.15	5.21	4.20	2.41	3.84	2.49	2.70	4.50	2.39
Total	**3.43**	**2.78**	**2.41**	**1.54**	**1.73**	**2.16**	**2.27**	**1.93**	**1.76**

a) AE/6, atomization energies; ABDE/4, Alkyl bond dissociation energy; EA/13, electron affinities; PA/8, proton affinities; HAT/6, Heavy atom transfer, NS/6, nucleophilic substitutions ; UA/6, unimolecular associations; HT/6, hydrogen transfer; HB/6 hydrogen bond; CT/7, charge transfer; DI/6, dipole interactions; WI7, weak interactions; PPS5, π-π stacking, SIE4x4, self-interaction error; IP/13, adiabatic ionization potentials; b) Please note that the MAEs of the AE/6 dataset reported in reference 7 are systematically divided by 4.83, which is the mean number of bonds per molecule in the dataset. This explains the apparent discrepancy between the data reported in the table and those listed in reference 7.

Figure captions

Figure 1. Dissociation energy profiles for the X_2^+ dimers (X=H, He, Ne and Ar). In all cases the zero energy reference is set to $E(X)+E(X^+)$.

Figure 2. Mean Absolute Deviations (MAD) for the benchmark on Ionization Potential from Kohn-Sham orbital energies (IPK/7), adiabatic Ionization Potential (IP/13) and Self-Interaction Error (SIE4x4). See text for details.

Figure 3. Ionization Potentials (IP) as functions of the size of the well separated He_n clusters (n=1-16).

Figure 4. Dissociation energy profiles for X_2 dimers (X= He, Ne and Ar).

Figure 5. Mean Absolute Deviations (MADs) for several benchmarks computed with the RSX-QIDH functional and its variant RSX-QIH(SCF) not containing the nonlocal PT2 contribution.

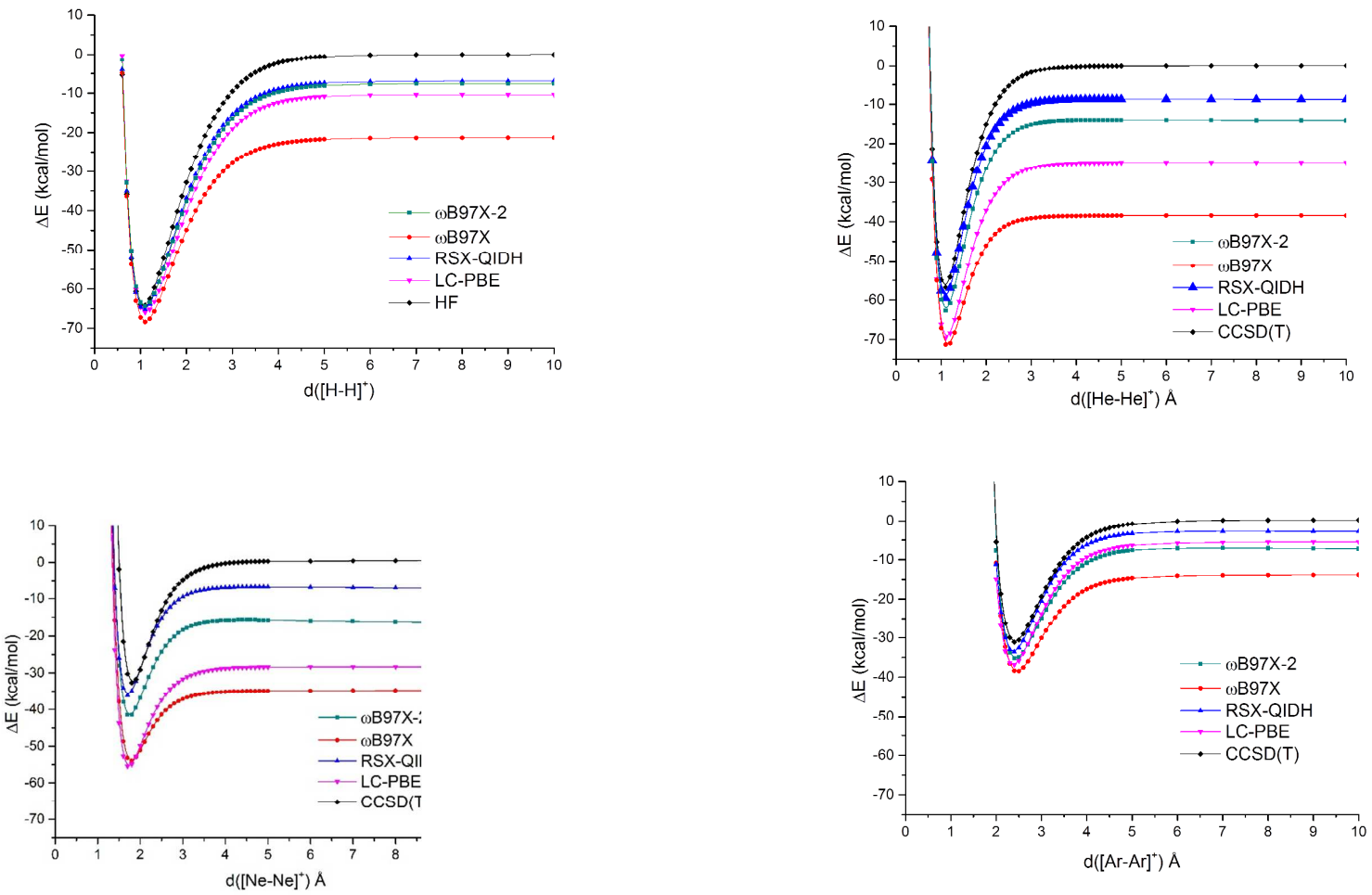
ΔE (kcal/mol)
d([H-H]+)
ωB97X-2
ωB97X
RSX-QIDH
LC-PBE
HF
d([He-He]+) Å
CCSD(T)
d([Ne-Ne]+) Å
d([Ar-Ar]+) Å

Figure 1

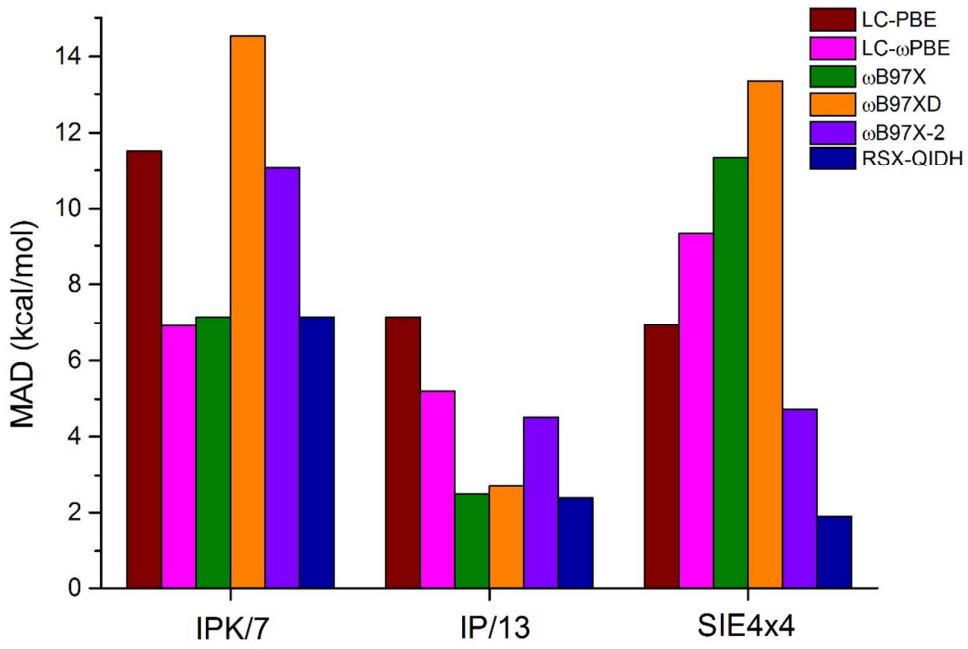
LC-PBE
LC-ωPBE
ωB97X
ωB97XD
ωB97X-2
RSX-QIDH
MAD (kcal/mol)
0
2
4
6
8
10
12
14
IPK/7
IP/13
SIE4x4

Figure 2

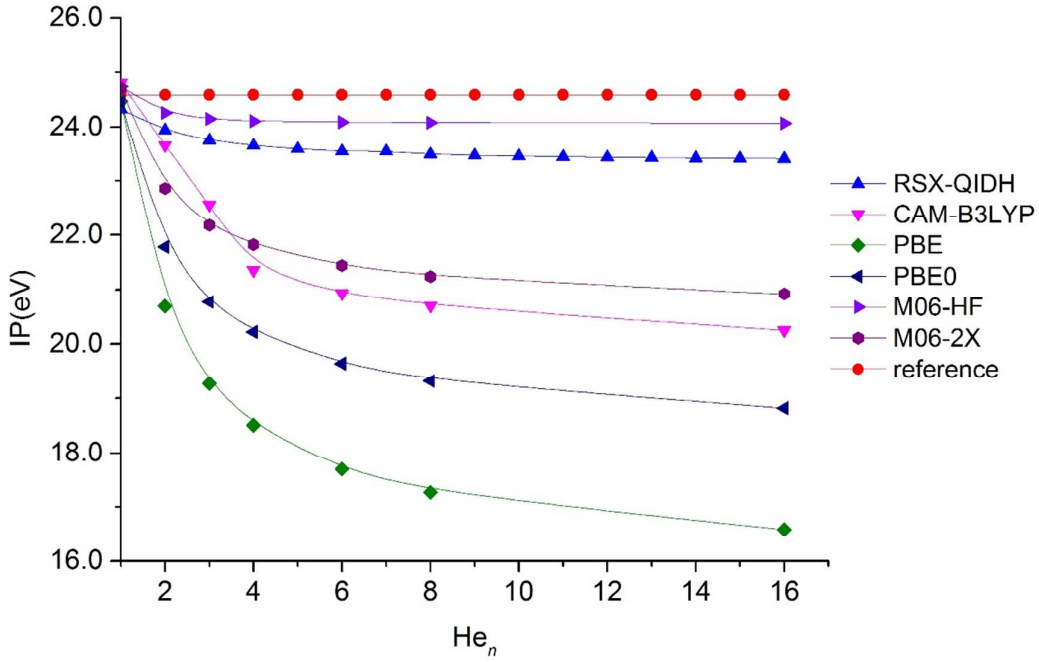
26.0
24.0
22.0
20.0
18.0
16.0
IP(eV)
2
4
6
8
10
12
14
16
He$_n$
RSX-QIDH
CAM-B3LYP
PBE
PBE0
M06-HF
M06-2X
reference

Figure 3

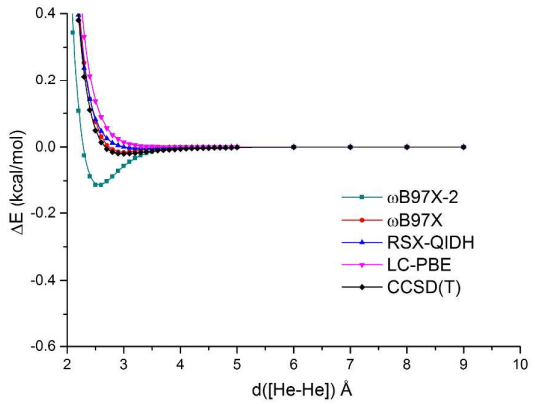
ΔE (kcal/mol)
d([He-He]) Å
ωB97X-2
ωB97X
RSX-QIDH
LC-PBE
CCSD(T)

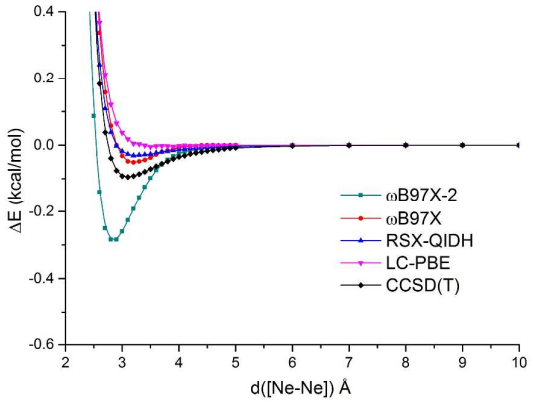
ΔE (kcal/mol)
d([Ne-Ne]) Å
ωB97X-2
ωB97X
RSX-QIDH
LC-PBE
CCSD(T)

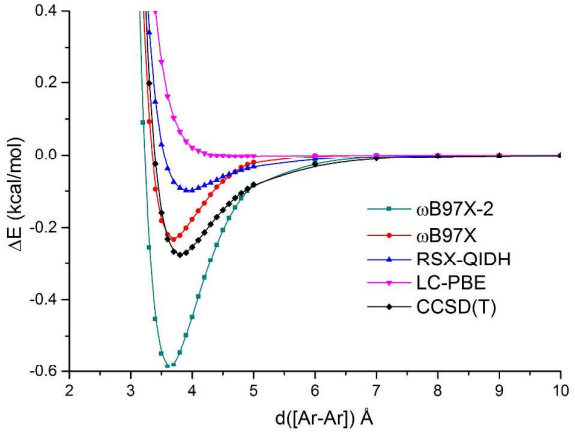
ΔE (kcal/mol)
d([Ar-Ar]) Å
ωB97X-2
ωB97X
RSX-QIDH
LC-PBE
CCSD(T)

Figure 4

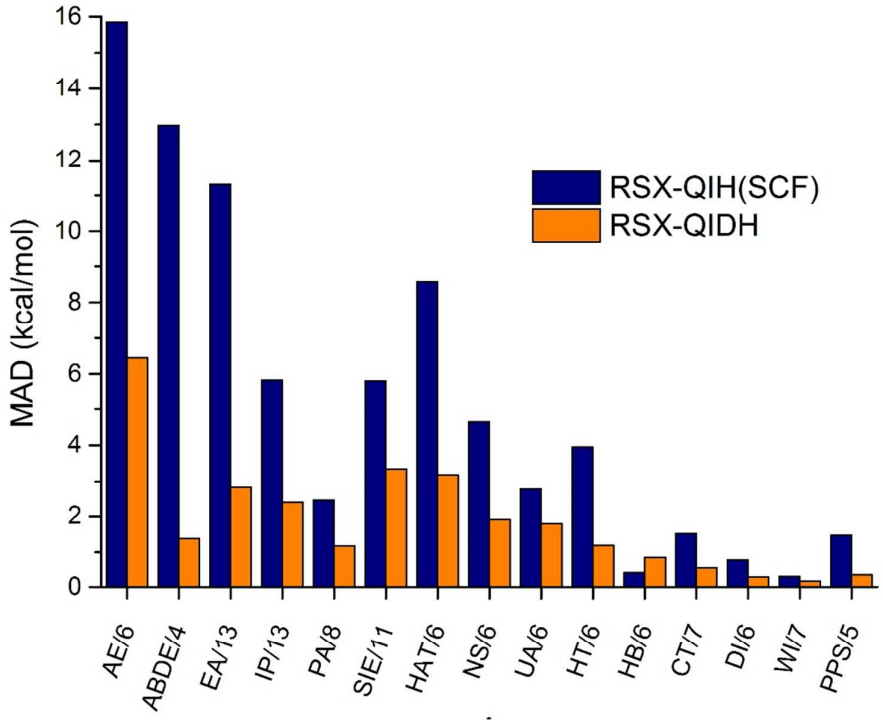
MAD (kcal/mol)
0
2
4
6
8
10
12
14
16
RSX-QIH(SCF)
RSX-QIDH
AE/6
ABDE/4
EA/13
IP/13
PA/8
SIE/11
HAT/6
NS/6
UA/6
HT/6
HB/6
CT/7
DI/6
WI/7
PPS/5

Figure 5

TOC Graphic